

# **Tribological, Thermal and Kinetic Attributes of Copper and Silicon Dioxide CMP Processes**

*Y. Zhuang, Z. Li, J. Sorooshian and A. Philipossian  
Department of Chemical and Environmental Engineering  
The University of Arizona, Tucson, AZ 85721, USA*

*L. Borucki  
Intelligent Planar, Mesa, AZ 85205, USA*

## Abstract

Experimental and numerical analyses of the tribological, thermal and kinetic attributes of silicon dioxide and copper CMP processes are presented in this study. Real-time friction forces are measured to determine the lubrication mechanism during copper polishing. Pad temperatures are simultaneously measured by an infrared camera and are shown to correlate with the copper removal rates. Different platen temperatures are applied during silicon dioxide polishing, ranging from 10 to 45 °C. Silicon dioxide removal rates are found to increase with the platen temperature and exhibit highly non-Prestonian behavior. Lim-Ashby plots, which show the separate effects of polishing pressure and wafer-pad sliding velocity, are used to describe the non-Prestonian copper and silicon dioxide removal rates. Assuming the chemical reaction temperature is determined by transient flash heating, a two-step modified Langmuir-Hinshelwood model is found to describe the copper and silicon dioxide removal rates well for the slurries used in this study. Extracted chemical and mechanical rate constants indicate that silicon dioxide removal can span a range of regimes from mechanically-limited to nearly equal balance between mechanical and chemical mechanisms; while for copper CMP, extracted mechanical rate constants exceed the chemical rate constants, suggesting that copper polishing is more chemically controlled.

## Introduction

Chemical mechanical planarization (CMP) has been widely employed to planarize interlayer dielectric and copper damascene structures in integrated circuit manufacturing processes. At the same time, there have been tremendous efforts in developing models to predict copper and silicon dioxide removal rates during the polishing process. These models can be classified into two categories: (1) ones that do not explicitly incorporate a chemical reaction mechanism [1-5] and (2) ones that include both chemical and mechanical aspects of polishing [6-8]. Most models in the first category are based on modifications of the Preston's equation. For example, Zhang and Busnaina developed a mechanical model, in which silicon dioxide removal rate is proportional to the square root of the product of polishing pressure and wafer-pad sliding velocity [1]. Recently, models that include both chemical and mechanical mechanisms have been proposed to predict copper and silicon dioxide removal rates [6-8]. With explicit chemical reaction mechanism, these models provide a better understanding of the synergistic work of the chemical and mechanical effects during the polishing process.

In this paper, experimental and numerical analyses on the tribological, thermal and kinetic attributes of copper and silicon dioxide CMP processes are presented. Real-time friction forces are measured to determine the lubrication mechanism during copper polishing. Pad temperatures are measured simultaneously to investigate thermal effects on copper removal rates. Lim-Ashby plots, which show the separate effects of polishing pressure and relative wafer-pad sliding velocity, are used to describe the non-Prestonian copper and silicon dioxide

removal rates. A modified two-step Langmuir-Hinshelwood model with explicit chemical and mechanical mechanisms is used to simulate the copper and silicon dioxide removal rates, as well as the chemical and mechanical dominance during the polishing process.

### Experimental conditions and results of copper polishing

A scaled version of a Speedfam-IPEC 472 polisher was used to polish blanket 4-inch copper wafers at the ambient temperature of 24 °C. Details of the experimental apparatus as well as its unique ability to acquire real-time shear force data critical for determining the coefficient of friction (*COF*) were described elsewhere [9-11]. Slurry used for copper polishing consisted of 1 volume part of Fujimi PL-7102 slurry, 9 volume parts of ultra pure water and 0.3 volume part of hydrogen peroxide (30 %). Prior to data acquisition, the IC-1000 K-groove pad was conditioned at the pressure of 0.5 PSI (3.45 kPa) for 30 minutes using ultra pure water by a 100-grit diamond disc which rotated at 30 RPM and oscillated at 0.33 Hz. Pad conditioning was followed by a 5-minute pad break-in with the slurry. The same rotational velocity and oscillation frequency were used for in-situ pad conditioning. Three polishing pressures (1.5, 2 and 2.5 PSI) and relative pad-wafer sliding velocities (0.31, 0.62 and 1.09 m/s) were used in this study. In all cases, slurry flow rate was kept constant at 80 ml/min. Two copper wafers were polished for 90 seconds at each polishing condition to confirm the experimental reproducibility. Pad surface temperature was recorded by an infrared camera which took five thermal images every second during polishing. Five locations outside the leading edge of the wafer carrier were selected to report the pad temperature and their values were averaged.

Figure 1 shows the Stribeck curve obtained for copper polishing. In the Stribeck curve, the coefficient of friction (*COF*) is defined as the ratio of the measured shear force to the applied normal force during the polishing process:

$$COF = \frac{F_{Shear}}{F_{Normal}} \quad (1)$$

The Sommerfeld number (*So*) is a dimensionless grouping of CMP-specific parameters defined as

$$So = \frac{\mu \cdot V}{p \cdot \delta} \quad (2)$$

where  $\mu$  is the slurry viscosity,  $V$  is the relative pad-wafer sliding velocity,  $p$  is the applied polishing pressure, and  $\delta$  is the effective fluid film thickness. The effective fluid film thickness ( $\delta$ ) is approximated as the pad surface roughness. Fig. 1 shows that the coefficient of friction (*COF*) remains relatively constant ranging from 0.60 to 0.70 as a function of the Sommerfeld number. This indicates that the dominant tribological mechanism for copper polishing in this study is that of ‘boundary lubrication’, in which abrasive particles, pad asperities and the surface of the wafer are all in direct contact with one another during polishing.

Figure 2 shows the pad temperature transients at different  $p \times V$  conditions during the copper polishing. The pad temperature transient is defined as the pad temperature increase due to the friction generated during the polishing process. The pad temperature transient generally increases with the polishing power ( $p \times V$ ) as expected. However, a drop of the pad temperature transient is observed when  $p \times V$  increases from 10,700 to 11,200 Pa-m/s.

Figure 3 shows the copper removal rates at different  $p \times V$  conditions in this study. Copper removal rates exhibit a non-Prestonian behavior as they do not increase linearly with the polishing power ( $p \times V$ ). The copper removal rates decrease significantly when  $p \times V$  increases from 10,700 to 11,200 Pa-m/s. The pad temperature transients also decrease at

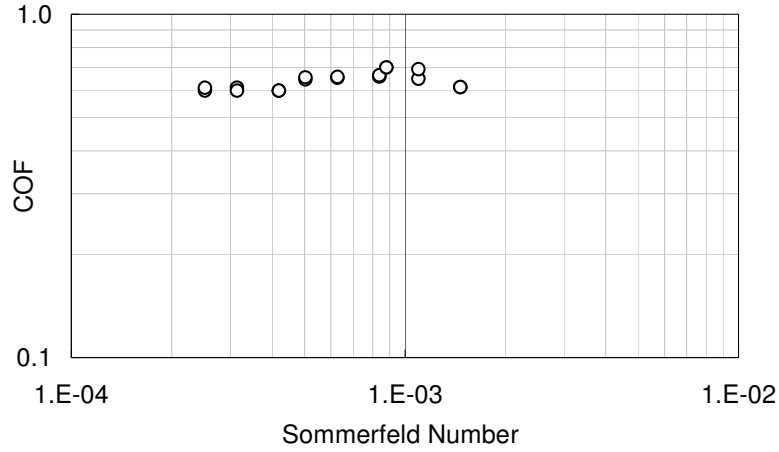


Figure 1. Coefficient of friction vs. Sommerfeld number during copper polishing

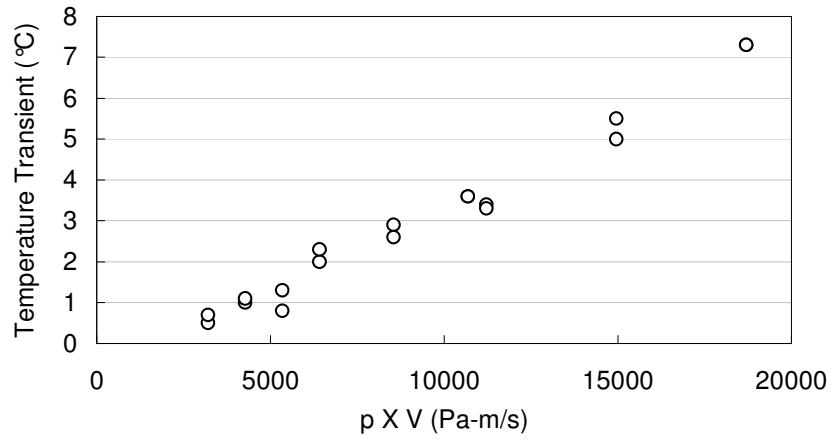


Figure 2. Pad temperature transients during copper polishing

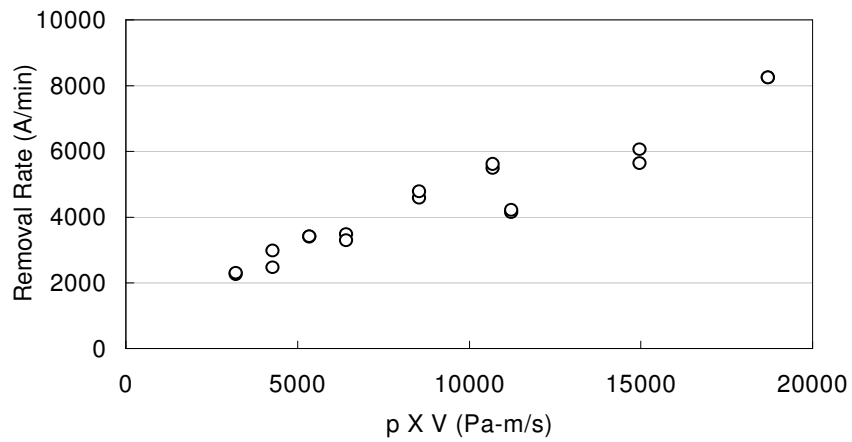


Figure 3. Copper removal rates at different p x V conditions

these polishing conditions as shown in Fig. 2, indicating a correlation between the copper removal rates and the pad temperature transients. Large pad temperature transient results in a hot pad and consequently a hot copper wafer, which in turn leads to enhanced oxidation reactions on the wafer surface and a high copper removal rate.

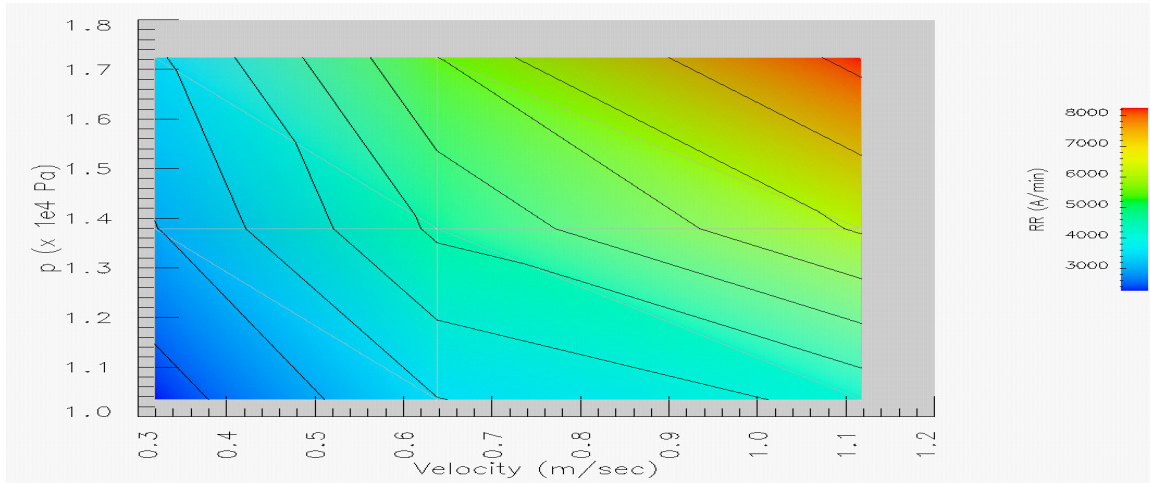


Figure 4. Lim-Ashby plot of copper removal rates

As the copper removal rates exhibit non-Prestonian behavior in this study, Lim-Ashby plot [12], an alternative to Preston plot, is used to describe the copper removal rates shown in Fig. 4. In the Lim-Ashby plot, contours of removal rates are plotted as a function of the polishing pressure ( $p$ ) on one axis and the relative pad-wafer sliding velocity ( $V$ ) on the other. Different from the Preston plot, the Lim-Ashby plot shows the separate influences of  $p$  and  $V$  rather than assuming a dependence of the removal rate solely on  $p \times V$  values. Therefore, the Lim-Ashby plot is capable of describing both Prestonian and non-Prestonian removal rates. In addition, compared with the Preston plot, the Lim-Ashby plot is a more powerful plot as it gives an estimate of the removal rate based on any individual  $p$  and  $V$  values rather than the grouped  $p \times V$  values.

#### Experimental conditions and results of silicon dioxide polishing

A Speedfam-IPEC Avanti-472 polisher was used to polish blanket 6-inch thermally grown silicon dioxide wafers. On the primary platen, polishing experiments were performed with an in-situ conditioning pressure of 0.5 PSI. Cabot D7300 fumed silica slurry (12.5 percent by weight) was used in conjunction with an IC-1400 K-grooved pad. The slurry flow rate was kept constant at 270 ml/min. The polishing pressures and relative pad-wafer sliding velocities ranged from 3 to 7 PSI, and from 0.5 to 1.5 m/s, respectively. Two wafers were polished for 180 seconds at each polishing condition to confirm the experimental reproducibility. Four different platen temperatures (10, 24, 35 and 45 °C) were applied during polishing. The platen temperature was controlled using the polisher's internal heat exchange system for platen heating and an external chiller for platen cooling.

Figure 5 shows the silicon dioxide removal rates under different platen temperatures in this study. The removal rates increase with the platen temperatures, particularly at high  $p \times V$  values, indicating the polishing process is thermally activated in this region. The silicon dioxide removal rates exhibit a highly non-Prestonian behavior, decreasing significantly when  $p \times V$  increases from 24,300 to 31,200 Pa-m/s, and from 41,600 to 52,100 pa-m/s. Figure 6 shows

the Lim-Ashby plot of the silicon dioxide removal rates at the platen temperature of 24 °C, which indicates that the oxide removal rates have a strong dependence on the polishing pressure and do not vary significantly with the wafer-pad sliding velocity. The Lim-Ashby plots of the silicon dioxide removal rates at other platen temperatures have similar contour patterns to that shown in Fig. 6 and thus are not shown here.

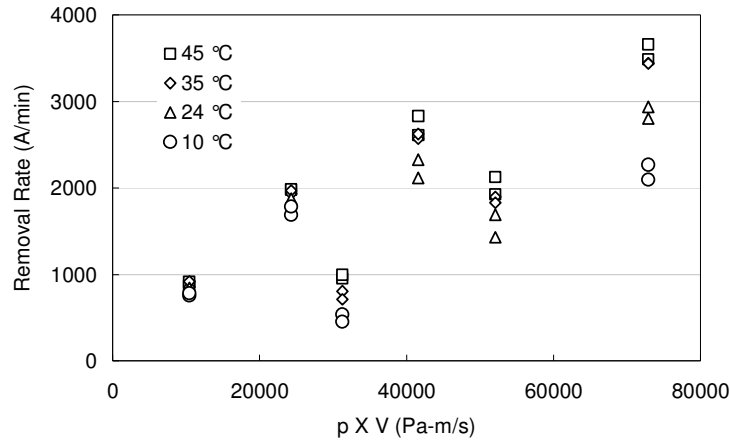


Figure 5. Silicon dioxide removal rates at different platen temperatures

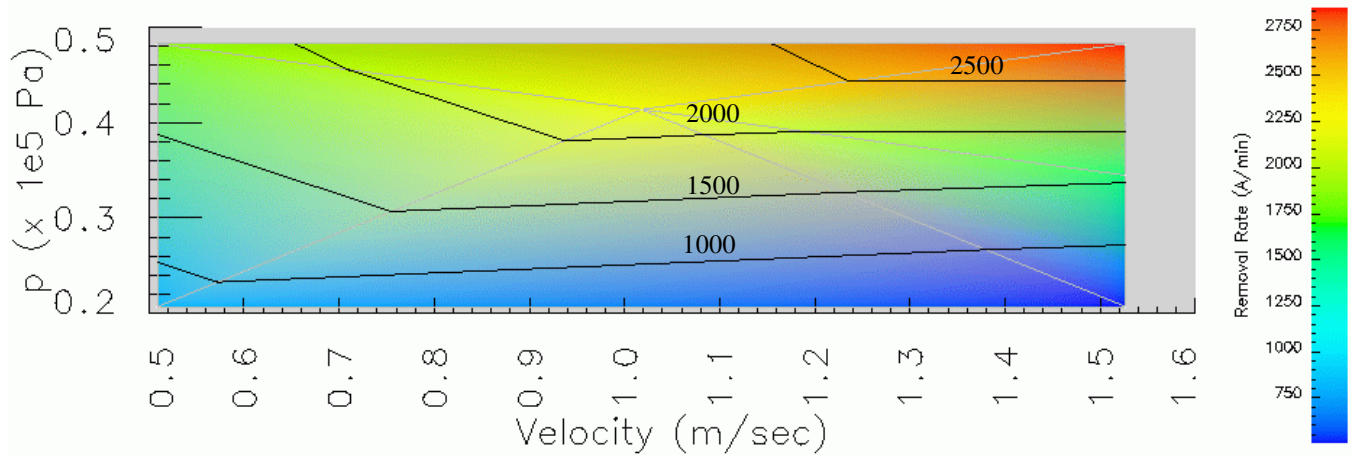


Figure 6. Lim-Ashby plot of silicon dioxide removal rates at platen temperature of 24 °C

### Numerical kinetic analysis

A modified two-step Langmuir-Hinshelwood model [7-8] is used to simulate the copper and silicon dioxide removal rates in this study. In this model, it is assumed that  $n$  moles of reactant  $R$  in the slurry reacts with the copper or silicon dioxide surface film ( $S$ ) at rate  $k_1$  to form a surface layer  $\underline{L}$ ,



This surface layer is then removed by mechanical abrasion with rate  $k_2$



The abraded material  $L$  is assumed to be carried away by the slurry and not re-deposited on the wafer surface. Assuming the rate of the surface layer formation is equal to the rate of its

depletion, the local removal rate in this sequential mechanism is

$$RR = \frac{M_w}{\rho} \frac{k_1 C_R^n}{1 + \frac{k_1 C_R^n}{k_2}} \quad (5)$$

where  $C_R$  is the local molar concentration of the reactant  $R$ . To simplify the model, it is assumed that there is no reactant depletion so that  $C_R$  remains constant in Equation (5). This allows  $C_R$  to be absorbed into  $k_1$  and its value is set to be unity. The chemical reaction rate constant  $k_1$  in Equation (5) is expressed as

$$k_1 = A \exp(-E / kT_w) \quad (6)$$

where  $A$  is an exponential factor,  $E$  is the activation energy,  $k$  is a gas constant ( $8.62 \times 10^{-5}$  eV/k), and  $T_w$  is the wafer temperature. The mechanical removal rate constant  $k_2$  in Equation (5) is expressed as

$$k_2 = C_p pV \quad (7)$$

where  $C_p$  is an assumed proportionality constant. Assuming the chemical reaction is determined by transient flash heating, the wafer temperature ( $T_w$ ) in Equation (6) is expressed as

$$T_w = T_a + \beta pV^{1-a} \quad (8)$$

where  $T_a$  is the ambient temperature,  $\beta$  is a grouping of parameters including the coefficient of friction, contact area fraction and associated pad properties, and  $a$  is an exponential factor. The derivation of Equation (8) is described in detail elsewhere [13]. During model simulation, parameters  $A$ ,  $C_p$ ,  $\beta$  and  $a$  are optimized to minimize the square of the error associated with the experimental and predicted values of the removal rates.

Figures 7 and 8 show the comparison of the experimental and simulated copper and silicon dioxide removal rates, respectively. The model successfully captures the drop of the copper and silicon dioxide removal rates with the polishing power ( $p \times V$ ).

Figure 9 shows the Lim-Ashby plot of simulated ratio of the chemical reaction rate constant to the mechanical removal rate constant ( $k_1/k_2$ ) for the copper polishing. The chemical reaction rate constant ( $k_1$ ) is smaller than the mechanical removal rate constant ( $k_2$ ), indicating that copper polishing is largely chemically limited in this study.

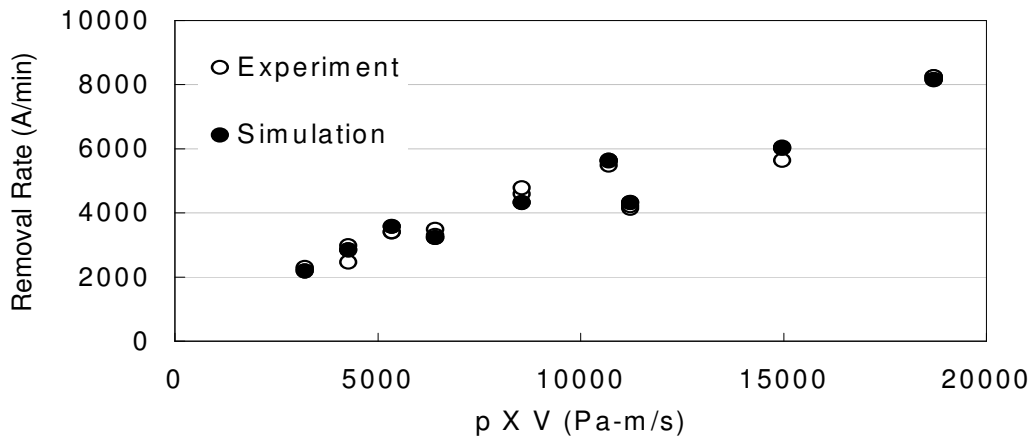


Figure 7. Comparison of experimental and simulated copper removal rates

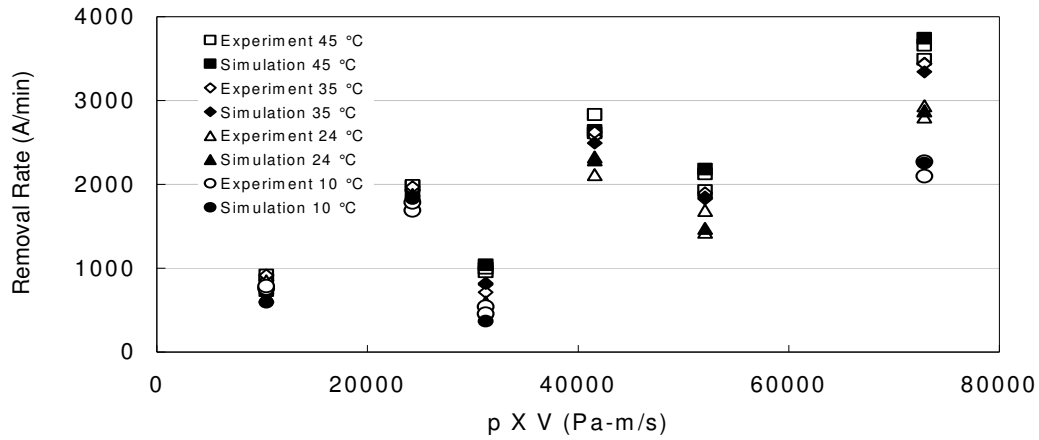


Figure 8. Comparison of experimental and simulated silicon dioxide removal rates

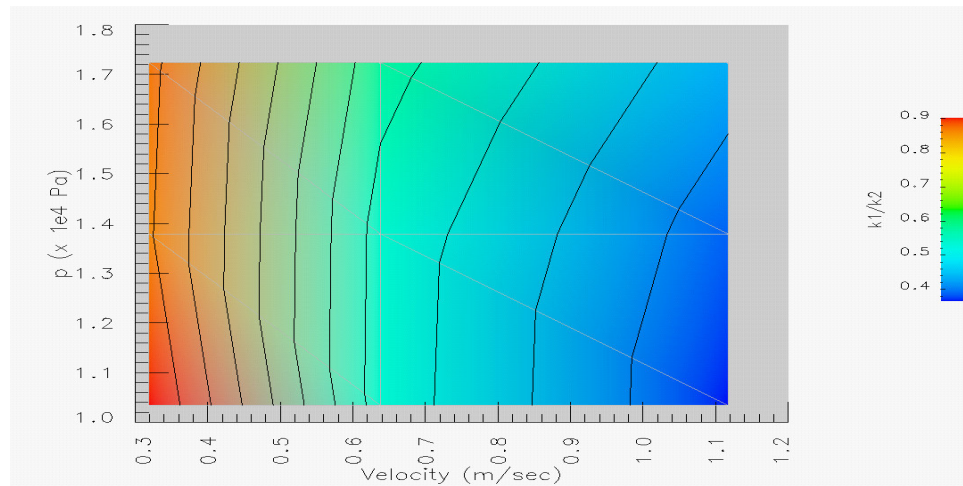


Figure 9. Lim-Ashby plot of  $k_1/k_2$  for copper polishing

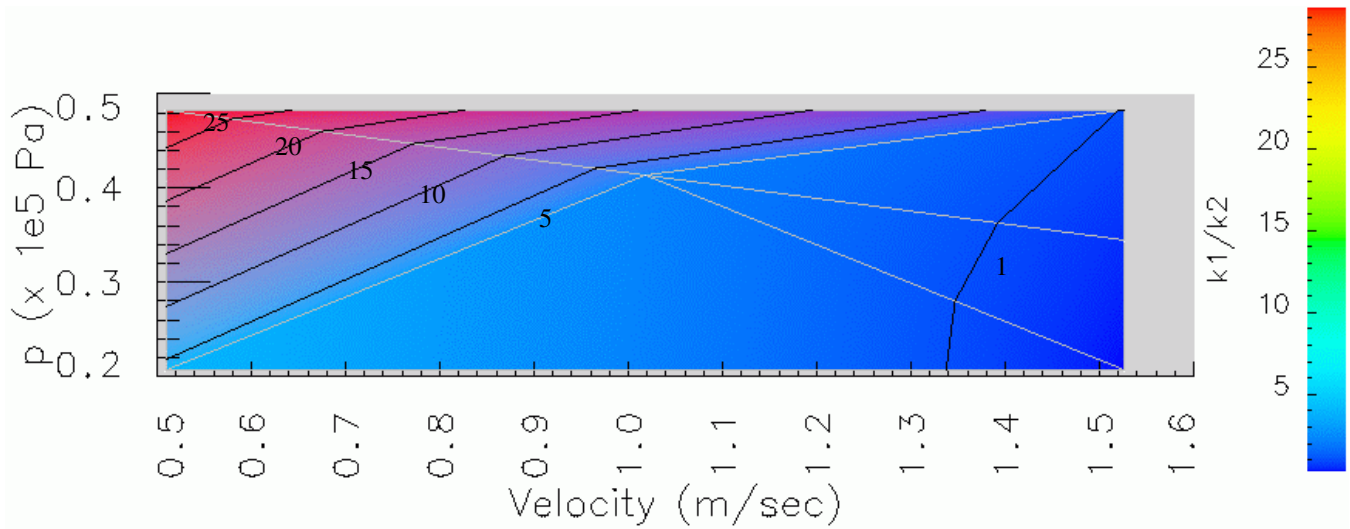


Figure 10. Lim-Ashby plot of  $k_1/k_2$  for silicon dioxide polishing at platen temperature of 24 °C

Figure 10 shows the Lim-Ashby plot of simulated ratio of the chemical reaction rate constant to the mechanical removal rate constant ( $k_1/k_2$ ) at the platen temperature of 24 °C for the silicon dioxide polishing. When the pad-wafer sliding velocity is lower than 1.3 m/s, the chemical reaction rate constant is larger than the mechanical removal rate constant, indicating the silicon dioxide polishing is mechanically limited in this region; while at high pad-wafer sliding velocity (1.5 m/s), the chemical rate constant is close to the mechanical rate constant, indicating a balanced chemical and mechanical mechanism. The Lim-Ashby plots of  $k_1/k_2$  at other platen temperatures have similar contour patterns to that shown in Fig. 10 and are not shown here.

## Conclusion

Recent studies on the tribological, thermal and kinetic attributes of copper and silicon dioxide CMP processes are presented. Results from the frictional study indicate that boundary lubrication is the dominant tribological mechanism for the copper polishing. Thermal study shows a correlation between the pad temperature transients and the copper removal rates, and the platen temperatures have a significant effect on the silicon dioxide removal rates. Both copper and silicon dioxide removal rates exhibit non-Prestonian behaviors. Lim-Ashby plots, which show the separate effects of polishing pressure and relative wafer-pad sliding velocity, are thus used to describe the copper and silicon dioxide removal rates. Assuming the chemical reaction temperature is determined by transient flash heating, a modified two-step Langmuir-Hinshelwood model is used to simulate copper and silicon dioxide removal rates. The model successfully simulates the decrease of copper and silicon dioxide removal rates with the polishing power. Simulated chemical and mechanical rate constants indicate that silicon dioxide removal can span a range of regimes from mechanically-limited to nearly equal balance between mechanical and chemical mechanisms; while for copper CMP, the mechanical rate constants exceed the chemical rate constants, suggesting that copper polishing is more chemically controlled.

## References

1. F. Zhang and A. Busnaina, *Electrochemical Solid-State Letters*, **1**, 184 (1998).
2. W. Tseng and Y. Wang, *Journal of the Electrochemical Society*, **144**, L15 (1997).
3. F. Shi and B. Zhao, *Applied Physics A – Materials Science and Processing*, **67**, 249 (1998).
4. B. Zhao and F. Shi, *Electrochemical Solid-State Letters*, **2**, 145 (1999).
5. Y. Homma, F. Fukushima, S. Kondo and N. Sakuma, *Journal of the Electrochemical Society*, **150**, G751 (2003).
6. C. Borst, D. Thakurta, W. Gill and R. Gutmann, *Journal of the Electrochemical Society*, **149**, G118 (2002).
7. D. Thakurta, D. Schwendeman, R. Gutmann, S. Shankar, L. Jiang and W. Gill, *Thin Solid Films*, **414**,78 (2002).
8. Z. Li, L. Borucki, and A. Philipossian, *Journal of the Electrochemical Society*, **151**, G482 (2004).
9. A. Philipossian and E. Mitchell, *Japanese Journal of Applied Physics*, **42**, 7259 (2003).
10. A. Philipossian and S. Olsen, *Japanese Journal of Applied Physics*, **42**, 6371 (2003).
11. A. Philipossian and E. Mitchell, *Journal of the Electrochemical Society*, **150**, G854 (2003).
12. S. C. Lim and M. F. Ashby, *Acta Metallurgica*, **35**, 1 (1987).
13. J. Sorooshian, L. Borucki, D. Stein, R. Timon, D. Hetherington and A. Philipossian, submitted to *Journal of Tribology* (2004).